

# An investigation of a wash-durable solar energy harvesting textile

Achala Satharasinghe  | Theodore Hughes-Riley  | Tilak Dias

Advanced Textiles Research Group, School of Art and Design, Nottingham Trent University, Bonington Building, Dryden Street, Nottingham NG1 4GG, UK

## Correspondence

Achala Satharasinghe, Advanced Textiles Research Group, School of Art and Design, Nottingham Trent University, Bonington Building, Dryden Street, Nottingham NG1 4GG, UK.

Email: achala.satharasinghe2016@my.ntu.ac.uk

## Funding information

Nottingham Trent University

## Abstract

This work demonstrates a novel and sustainable energy solution in the form of a photovoltaic fabric that can deliver a reliable energy source for wearable and mobile devices. The solar fabric was woven using electronic yarns created by embedding miniature crystalline silicon solar cells connected with fine copper wires within the fibres of a textile yarn. This approach of integrating solar energy harvesting capability within the heart of the textile fabric allows it to retain the flexibility, three-dimensional deformability, and moisture and heat transfer characteristics of the fabric. In this investigation, both the design and performance of the solar cell embedded yarns and solar energy harvesting fabrics were explored. These yarns and resultant fabrics were characterised under different light intensities and at different angles of incident light, a critical factor for a wearable device. The solar cell embedded yarns woven into fabrics can undergo domestic laundering and maintained ~90% of their original power output after 15 machine wash cycles. The solar fabric embedded with 200 solar cells demonstrated here (44.5 mm × 45.5 mm active area) was capable of continuously generating ~2.15 mW/cm<sup>2</sup> under one sun illumination and was capable of powering a basic mobile phone. The power generation capability and durability of the solar energy harvesting fabric proved its viability to power wearable devices as an integral part of regular clothing.

## KEYWORDS

electronic textiles, energy harvesting, photovoltaic textile, smart textiles, solar energy, washable, wearable devices

## 1 | INTRODUCTION

This work presents a novel photovoltaic (PV) textile, which has been designed to provide a sustainable and fully embedded energy solution for wearable and mobile electronic devices. The PV textiles convert solar energy into electricity using a network of discrete miniature solar cells (SCs) embedded within the fibres of the textile, creating an

aesthetically pleasing, conformable, and wash-durable device. The paper analyses the energy harvesting performance of PV elements embedded within textile structures (yarns and fabrics) in relation to their construction (yarn components and the fabric surrounding) and operating conditions (incident light intensity and angle, deformations, washing, abrasion, and wetting) that would be experienced by the fabric when applied to real-life applications.

This is an open access article under the terms of the Creative Commons Attribution License, which permits use, distribution and reproduction in any medium, provided the original work is properly cited.

© 2019 The Authors. Progress in Photovoltaics: Research and Applications published by John Wiley & Sons Ltd

The emergence of wearable devices, for applications including non-invasive health care monitoring,<sup>1</sup> sports,<sup>2</sup> learning assistance,<sup>3</sup> and entertainment,<sup>4</sup> has been catalysed by the miniaturisation of electronic components and low power-consuming devices. Despite the unprecedented interest and potential foreseen, the Achilles heel of many wearable and electronic textile (E-textile) devices are their energy requirement, which is a major hurdle to the wider adoption of E-textiles.<sup>5,6</sup> Most commercially available wearable systems are powered by standard solid coin cells, pouch cell, cylindrical cell, or prismatic cell batteries of alkaline, nickel metal hydride (NiMH), lithium-ion (Li-ion), or lithium-ion polymer (LiPo) type.<sup>7</sup> These batteries are typically attached to the garment after assembly or embedded in a removable module, making the systems bulky and cumbersome to use.<sup>8</sup> Smaller and lighter batteries require frequent recharging. In light of these drawbacks, many have proposed integrating energy harvesting capability into clothing,<sup>9,10</sup> to power wearable devices using ambient energy available from the surrounding.

Amongst the other energy harvesting technologies explored for E-textiles, such as tribo-electric,<sup>11,12</sup> piezo-electric,<sup>13,14</sup> thermoelectric,<sup>15</sup> or electromagnetic induction,<sup>16</sup> solar energy harvesting has been one of the most investigated avenues due to the abundance of solar energy<sup>17</sup> and the maturity of PV technologies.<sup>18</sup> Various approaches to integrate solar energy harvesting capability into textiles have seen a rapid growth during the last two decades<sup>19-21</sup>: The first attempts were to superficially attach rigid<sup>22</sup> or flexible<sup>23</sup> solar panels onto fabrics; these were limited to functional clothing and futuristic fashion prototypes and were far from the appearance, feel, and durability of regular clothing. Printing,<sup>24</sup> laminating,<sup>25</sup> or coating<sup>26</sup> of organic PVs (OPVs),<sup>27</sup> and hybrid PV such as dye-sensitised solar cells (DSSC)<sup>28</sup> and perovskite SCs<sup>29</sup> onto textile substrates have dominated most of the textile-based PV research. Thin film PV laminates such as copper indium gallium diselenide (CIGS)<sup>30</sup> and amorphous thin-film silicon (a-Si, TF-Si)<sup>31</sup> have also been extensively explored for textile applications. In addition to the inherent flexibility, a preference towards OPVs, hybrid PVs, and thin film PVs have emerged due to their affordability and recent improvements in efficiency; however, it is important to note that these solutions are still incapable of matching the efficiencies of inorganic cells<sup>32</sup>. Despite being inherently flexible, the monolithic, large-area, nonporous structure of these PV systems significantly changes the appearance and feel of the textile and restricts the shear behaviour and air permeability of the textile substrate, making them uncomfortable and less appealing to the wearer. An alternative solution is to weave PV-coated wires<sup>33,34</sup> or flexible PV tapes<sup>27,35</sup> of DSSC type,<sup>36,37</sup> perovskite type<sup>38,39</sup> or OPV<sup>40,41</sup> into fabrics, which has also been widely explored for wearable applications. In principle, the PV layers of these wires or tapes were similar to the coated, laminated or printed films discussed earlier, with the small cross sections and large aspect ratios of these wires or tapes allowing them to be woven into fabrics. Fabrics woven with PV-coated wires or flexible PV tapes showed improvements in the shear behaviour and breathability; however, they still looked and felt significantly different from normal textile fabrics.

In general, the majority of PV-textile systems have not reported the compatibility with water or washing. Two recent studies on elastomer-coated organic PV<sup>42</sup> and textile-based polymer SCs<sup>43</sup> show some evidence of durability to detergent-water mixtures. In these studies, free-standing organic PV cells enhanced with liquid barrier laminates were tested inside a small beaker of stirred water-detergent mixture for 10 to 30minute cycles. However, these mild test conditions are far from the rigorous hydro-mechanical agitation undergone by regular clothing in a domestic washing machine.

The solar energy harvesting fabric demonstrated here was constructed by weaving textile yarns embedded with miniature SCs (solar-E-yarns). To achieve a drapable and soft fabric that can endure machine washing, the shear behaviour and a low bending rigidity of the structure had to be maintained. Therefore, the rigid PV elements were deployed in a discontinuous fashion within the fabric in yarn form by employing electronic yarn technology.<sup>44</sup> Electronic yarns have previously seen small electronic chips integrated into the core of a textile yarn to add electronic functionality including illumination,<sup>45</sup> temperature sensing,<sup>46</sup> vibration sensing,<sup>47</sup> light sensing,<sup>48</sup> and acoustic sensing.<sup>49</sup>

The E-yarns with embedded SC (solar-E-yarns) were realised in three steps. First, miniature (1.5 mm × 3.0 mm × 0.2 mm) SCs were soldered in parallel onto two multistrand copper wires before being individually encapsulated within clear, cylindrical resin micropods. The solar-cell-micropod filament containing the encapsulated cells was then covered by a fibrous textile sheath to give the final solar-E-yarn a textile feel and appearance. The discrete micropods and the fibrous sheath provided the solar-E-yarns with a low bending rigidity and a high degree of porosity enabling the transfer of moisture and heat through the E-yarns, and resultant fabrics. This feature was crucial to prevent discomfort to the user caused by thermal and sweat build-up, especially during warm and sunny conditions.<sup>50</sup> The textile sheath also allowed the yarn to take any colour without significantly altering its optoelectronic performance. This method is applicable for embedding different types of SCs (including organic,<sup>51</sup> thin-film, perovskite<sup>52</sup> or multijunction<sup>53</sup> SCs) within textiles; however, this paper focuses on crystalline silicon (c-Si) type SCs given their high efficiencies.

A solar energy harvesting fabric demonstrator was woven using 20 solar-E-yarns embedded with 200 miniature SCs (10 per yarn) creating a photoactive area of 44.5 mm × 45.5 mm. The solar energy harvesting fabric generated an open circuit voltage ( $V_{OC}$ ) of 5.14 V, a short-circuit current ( $I_{SC}$ ) of 14.14 mA, and a maximum power output ( $P_{MAX}$ ) of 43.4 mW, with a 2.15 mW/cm<sup>2</sup> power density under one sun illumination (100 mW/cm<sup>2</sup>): This significantly exceeded the power densities for similar textile-like solar energy harvesting solutions reported such as the all-solid tailorable energy textile developed by Chai et al,<sup>37</sup> which generated ~1 mW/cm<sup>2</sup>, or the microcable power textile developed by Chen et al,<sup>54</sup> which generated 25 μW/cm<sup>2</sup>.

The integration of SCs within the E-yarn structure (first the micropod and then the fibrous sheath) will have an effect on the embedded SC performance,<sup>48</sup> and therefore, this was important to

analyse and understand. Voltage and current outputs have been presented at each stage of the E-yarn production process. Further data have been presented for solar-E-yarns with different colours of outer covering fibres. Similarly, the performance of the solar energy harvesting fabric was assessed under different incident light intensities, with further experiments conducted when the fabric underwent mechanical deformation. Since the solution was mainly intended for outdoor wearable applications, the evaluations were conducted between 100% and 25% of one sun intensities.

A critical factor to understand for a solar energy harvesting solution for a wearable application is how the angle of incident light effects the functionality of the device: ultimately a wearer of a solar energy harvesting device would move relative to the light source (i.e. the Sun). The performance as a function of the incident angle of the light has been characterised for solar-E-yarns both free-standing (the solar-E-yarn on its own and not embedded within a fabric) and in fabric form (woven into fabrics).

The solar-E-yarns woven into fabrics were assessed for their wash durability, with both hand washing and machine washing explored (in a domestic washing machine with a 2kg washing load). Resistance to abrasion was also evaluated. Solar-E-yarns were also assessed under wet conditions.

Finally, the ability of the solar energy harvesting fabric demonstrator to charge various energy storage devices (such as batteries and supercapacitors) was assessed.

This unique approach of embedding solar energy harvesting capabilities within textiles will revolutionise the way in which wearable and mobile electronic devices will be powered in the future. This technology allows for the creation of a solar energy harvesting fabric where the end user will not have to compromise on reusability, appearance, or comfort.

## 2 | MATERIALS AND METHODS

### 2.1 | Fabricating solar cell embedded yarns

To create the solar-E-yarns, miniature c-Si SCs with dimensions of 1.5 mm × 3.0 mm × 0.2 mm were sourced (Solar Capture Technologies, UK); the required dimensions were achieved by laser cutting standard laser grooved buried contact type c-Si SCs (cutting conducted by Solar Capture Technologies). The miniature SCs were soldered onto two fine copper (Cu) wires (seven strand, linear density = 120 mg/m, single strand diameter = 50 μm, electrical resistance = 1.35 Ω/cm; Knight Wire, UK), with Sn<sub>96.5</sub>Ag<sub>3.0</sub>Cu<sub>0.5</sub> solder paste (SolderPlus S965D500A6, Nordson EFD, UK) using a focussed IR spot reflow soldering device (PDR IR-E3 Rework System, PDR—Design & Manufacturing Centre, UK). Excess Cu lengths were removed after soldering. Cu wires were selected as interconnects due to their high electrical conductivity, cost-effectiveness, and excellent solderability using Pb-free soldering (further details of the soldering process are provided in Section S1). The  $I_{SC}$  and  $V_{OC}$  of the SCs before and after soldering onto Cu wires confirmed an

insignificant change in  $V_{OC}$  and ~5% reduction in  $I_{SC}$  after soldering (information on the effect of soldering on bare SCs provided in Section S5). The reduction in  $I_{SC}$  may be caused by the contamination of the photoactive surface by residues of the soldering process. The  $V_{OC}$  of the maiden miniature SC (SC before soldering) exhibited significantly lower values compared with the  $V_{OC}$  values for the original standard sized c-Si SC from which the miniature SC was cut. This may have been due to the increased edge recombination caused by increasing the area/perimeter ratio of the miniature cell.<sup>55</sup> The edge recombination can be minimised by enhancing passivation at the edges of the miniature cells<sup>56</sup>; however, this would need to be conducted at the cell fabrication stage.

The soldered SC–Cu filament was paired with a strong Vectran yarn (20 filaments, 100 denier, Vectran, Kuraray America Inc, USA) and positioned inside of a clear silicone tube (i.d. = 1.6 mm; Advanced Fluid Solutions Ltd, UK). The longitudinal centre axis of the SC (ie, centre of the 1.5-mm dimension) was positioned coincident with the centre axis of the silicone tube. A predetermined volume (~8 μL) of UV curable, optically clear resin (Dymax, 9001-E-V3.5, Dymax Corporation, USA) was injected into the silicone tube to fully encapsulate the SC: This resulted in a micropod length of approximately 4.0 to 4.5 mm (0.50–0.75 mm longer than the length of the SC on each side). The silicone tube containing the resin was exposed to a UV light source (BlueWave 50, Dymax Corporation, USA) for 60 seconds to fully cure the resin, forming a solid resin micropod. Finally, the cured resin micropod, with the SC (referred to as the solar-micropod filament hereafter), was pulled out of the silicone tube by applying a tensile force to the Vectran yarn (Figure 1).

The resultant solar-micro-pod filament was fed into a small diameter circular warp-knitting machine (RIUS MC-Knit braiders with 2.0-mm inner diameter hollow cylinder and six latch needles; RIUS, Spain) that was used to form the fibrous sheath around the solar-micropod filament. The first set of white polyester (PE) filament yarns (six 48f/167 dtex yarns) were delivered to the knitting needles on the outer surface of the needle cylinder and formed the circular knit braided structure. A second set of white PE filament yarns (four 48f/167 dtex yarns) were supplied directly through the inside of the hollow needle cylinder along with the solar-micropod filament (without making loops); these filament fibres were used to hold the solar-micropod filament co-axially inside of the knit-braided outer sleeve, creating the final solar-E-yarn (Figure 1B(iii)). For the red- and black-coloured solar-E-yarn experiments, PE filament yarns (six 48f/167 dtex yarns) of red and black colour were used for the knit-braid. A cross-sectional view of the solar-E-yarn is shown in Figure 1A.

For electrical characterisation and durability tests, solar-E-yarns with a single SC per yarn were fabricated. To construct the SC embedded demonstrator fabric, solar-E-yarns were fabricated with 10 SCs per yarn (Figure 2A). The 10 SCs were individually soldered in parallel onto a pair of Cu wires (with 2.0-mm gaps between adjacent cells), individually encapsulated within 4.0-mm-long resin micropods and covered inside of a white fibrous sheath using the same

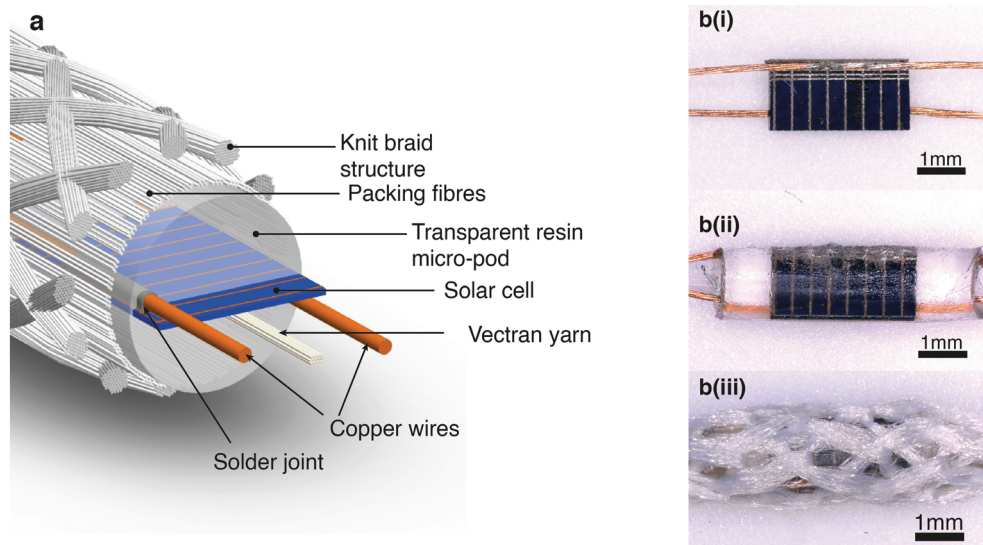


**FIGURE 1** Solar cell embedded yarn structure, fabrication process. (A) Schematic of the structure of the solar cell embedded yarns (solar-E-yarns). (B (i)) 1.5 mm × 3.0 mm × 0.2 mm solar cell soldered onto two, seven strand (50- $\mu$ m-diameter strands) copper wires. (B (ii)) The soldered solar cell embedded inside of a cylindrical, clear resin micropod of 1.6-mm diameter. (B (iii)) The solar-micro-pod filament covered by a fibrous sheath [Colour figure can be viewed at [wileyonlinelibrary.com](http://wileyonlinelibrary.com)]

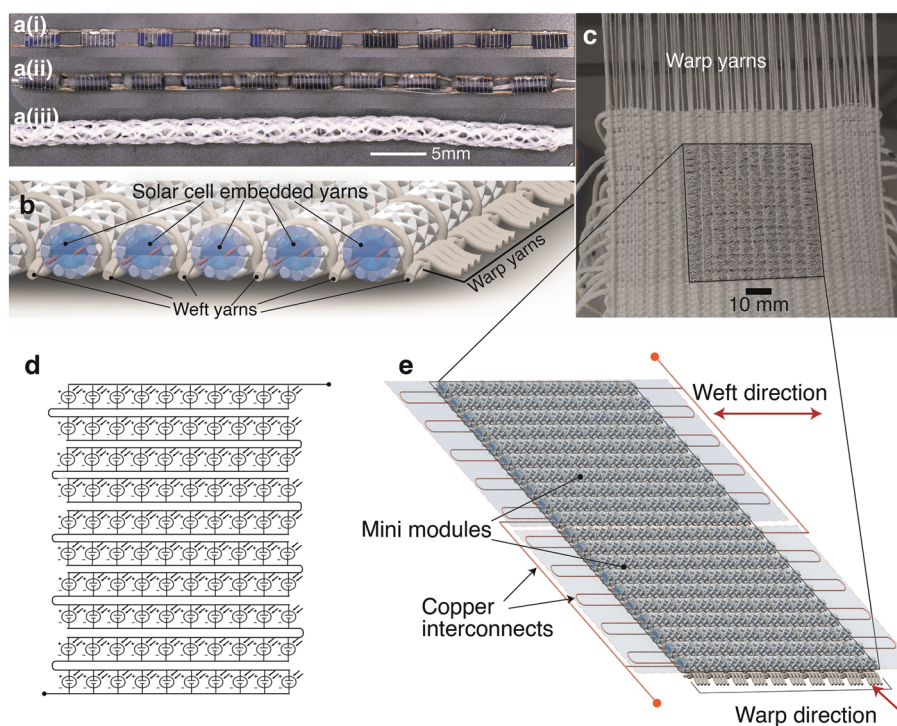


**FIGURE 2** Structure of solar cell embedded fabric demonstrator. (A (i)) 10 solar cells soldered in parallel onto two fine copper wires. (A (ii)) Soldered solar cells individually encapsulated within cylindrical resin micropods. (A (iii)) The encapsulated solar-micropod filament covered by a fibrous sheath. (B) Schematic of the cross-sectional view of the woven fabric with solar cell embedded yarns. (C) Image of the solar cell embedded fabric (black box indicating solar cell footprint). (D) Electrical circuit diagram of a minimodule made with 10 solar-E-yarns. The demonstrator fabric consisted of two minimodules. (E) Schematic of the solar cell fabric demonstrator showing how the solar-E-yarns and minimodules were connected [Colour figure can be viewed at [wileyonlinelibrary.com](http://wileyonlinelibrary.com)]

materials and procedures described above. The parallel networking of the cells allowed for current multiplication within each yarn; it was not desirable to solder in series and multiply the

voltage, as most wearable devices have low voltage requirements. The structural features of the parallel connection between SCs provided the solar-E-yarn a high tensile strength (with two Cu wires)

while ensuring the unifacial orientation of SCs within the solar-E-yarn.

## 2.2 | Creating solar cell embedded fabrics

To construct the SC embedded demonstrator fabric, 20 solar-E-yarns with 10 SCs per yarn were used: A woven fabric was created using these solar-E-yarns inserted in the weft direction (Figure 2B,C). A table top weaving loom (four shafts, 24" width; Harris Looms, UK) was prepared with 12-cm-wide sheet of warp yarns (10 yarns per centimetre) using white cotton yarns (38.9 × 2 tex; Elton Vale Yarns Ltd, UK). The warp yarns were threaded to achieve a four by one shedding pattern (a basket weave), as shown in Section S2. The solar-E-yarns were inserted in such a manner that the photoactive side was fully exposed on the front surface of the fabric. Cotton yarns (same type used for the warp) were used as weft yarns to fill the gaps between solar-E-yarns. In the case of demonstrator fabric (Figure 2B), one cotton weft yarn was inserted between each of the solar-E-yarns. To assess the effect of incident angle, fabrics with different spacings between the solar-E-yarns were made. A gap of 1.0 mm was achieved by inserting three cotton weft yarns between solar-E-yarns, and 3.0-mm gap was achieved by inserting seven cotton weft yarns between the solar-E-yarns. When required, knit braided yarns (with packing yarns and the knit braid only but without a solar-micropod filament) were used as the weft yarns along with cotton yarns, to add extra length to the fabric samples.

Two minimodules, each consisting of 10 solar-E-yarns, were created by connecting 10 solar-E-yarns in series, as shown in the circuit diagram in Figure 2D. The SC embedded fabric demonstrator (Figure 2E) was realised by wiring the minimodules in parallel (see Section S4 for further information). The SC embedded region of the fabric (the photoactive area) had a footprint of 44.5 mm × 45.5 mm (Figure 2C).

## 2.3 | Characterisation of solar cell embedded yarns and fabrics

For electrical characterisation of the solar-E-yarns and demonstrator fabric, two light sources were employed. For the majority of the experiments in this work, ABA type solar simulator (LSH-7320, Newport Corporation, UK) was used, with the exception of the incident angle varied measurements for the free-standing solar-E-yarns. For this experiment, a bespoke optical test rig with a tungsten halogen lamp (described in Section S3) was employed.

Electrical measurements were taken using a high precision digital multimeter (Model 34410A 6 ½, Agilent Technologies LDA UK Limited, UK). Unless otherwise stated, one sun intensity (100 mW/cm<sup>2</sup> with an AM1.5 G spectrum) was selected on the solar simulator for measurements. All fixed angle measurements were conducted at a temperature maintained at 25 ± 1 °C using a feedback controlled cooling system (described in Section S3).

For  $I_{SC}$  measurements of solar fabrics under different incident light angles, a rotary sample holder was devised, with a goniometer (with 5°

increments). The rotary sample holder was mounted horizontally onto a vertical pole using an axle fixed through the rotary axis of the holder, allowing the angle of the sample holder to be varied relative to a horizontal plane.

To generate IV curves, a simple decadic resistor network (1 Ω – 100 MΩ) was built using fixed resistors (RS Components, UK). For each data point, the voltage and the electrical resistance across the resistor network was measured to calculate the corresponding current and power values. The maximum power point was realised to the accuracy of ±10 Ω.

All metallic components used in the experimental setups were covered with black nonreflective coatings or tapes. Additional details of the instruments and methods used for characterisation are included in Section S3.

## 2.4 | Liquid moisture management test

A control fabric woven using knit-braided yarns without solar-micropod filaments (all other material and process parameters remaining identical to the solar-E-yarns) was prepared (using an identical woven structure, process parameters, and additional cotton yarns similar to the demonstrator fabric) for a comparison test.

The SC embedded demonstrator fabric containing 200 SCs and the control fabric were tested using the Gravimetric Absorbance Test System (GATS—M/K systems Inc, USA; see Section S4). The backsides of the fabrics were covered by a thin polyethylene film with a 45 mm × 45 mm window, to expose the cell embedded area of the fabric to the porous plate of the GATS. The fabrics were placed on the porous plate of the GATS, and the absorption test was conducted with distilled water, until each fabric was saturated. The same steps were repeated for the control fabric.

## 2.5 | Durability testing

For durability testing, 15 identical solar-E-yarns were woven into three sets of fabric samples (five yarns per fabric), with 10-mm gaps between each adjacent solar-E-yarns. The first set of solar-E-yarns were machine washed in a domestic washing machine (Bosch Logixx 8 VarioPerfect, BSH Home Appliances Ltd, UK) with 20 g of detergent (Persil Non Bio, Unilever UK Ltd, UK) and line dried inside of a wash bag for 25 cycles (total washing time of 15 hours) along with ballasts (to create a total wash load of 2 ± 0.01 kg). This washing process closely followed the test procedure 4N outlined in the British standard BS EN ISO 6330:2012; *Textiles—Domestic washing and drying procedures for textile testing*.<sup>57</sup>

The second set of solar-E-yarns were hand washed with 10 g of detergent and line dried (drying was accelerated with a domestic cooling fan) for 25 cycles (total washing time of 7.5 hours), by closely following the AATCC Monograph M5 for Standardization of Hand Laundering for Fabrics and Apparel.<sup>58</sup> The washing and rinsing were conducted with 50 ± 2°C tap water (recorded using a digital temperature meter).

The third set of solar-E-yarns was subjected to abrasion testing using an abrasion tester (902 Mini Martindale, James Heal Ltd, England) for 6000 abrasion cycles according to *BS EN ISO 12947-2:2016*.<sup>59</sup> Microscopic images were taken before the start of the tests and after every 1000 cycles while the test sample was fixed to the abrasion tester.

A fourth set of five solar-E-yarns were prepared with enamelled seven-strand copper wires with a nylon sheath (BXL2001, OSCO Ltd, UK), instead of the multistrand copper wire (used in previous experiments). These were woven into a fabric similar to those used for the other durability tests. These solar-E-yarns were characterised after soaking with, and immersing in, tap water at room temperature ( $\sim 20^{\circ}\text{C}$ - $25^{\circ}\text{C}$ ) for 30 minutes.

The solar-E-yarns in the fabric samples were characterised for output current and voltage under standard one sun ( $100\text{ mW}/\text{cm}^2$ , AM 1.5 G spectrum) illumination before and after they have been subjected to the above described durability testing.

Further details of the sample preparation and test conditions are provided in Section S4.

### 3 | RESULTS AND DISCUSSION

#### 3.1 | Solar cell embedded yarns

The fabrication of solar-E-yarns involves three steps, soldering, encapsulation, and covering in fibres. After each step of production, the

electrical characteristics of the SCs were determined, and the results are shown in Figure 3A,B. The  $I_{\text{SC}}$ ,  $V_{\text{OC}}$ ,  $P_{\text{MAX}}$ , and fill factor (FF) values derived from the curves (Figure 3C(i)-(iv)) showed the changes in optoelectronic output due to the fabrication process. The linear relationship between light intensity and  $I_{\text{SC}}$  explains the clear change in  $I_{\text{SC}}$  during the yarn fabrication process. On the other hand,  $V_{\text{OC}}$  showed a modest change due to its logarithmic relationship with light intensity.<sup>60</sup> Therefore,  $I_{\text{SC}}$  can be considered as the parameter, representative of the amount of light flux received by the embedded SC.

When the SCs were encapsulated within the resin micropods, the  $I_{\text{SC}}$  and  $P_{\text{MAX}}$  values increase by 18.3% and 21.7%, respectively, due to the convergent (lensing) and light trapping effects by the micropod. A previous study<sup>48</sup> has investigated the performance of photodiodes embedded within small resin micropods; the effect of size, geometry, and optical properties of the micropod, along with the position of the device within the micropod, were estimated using a theoretical model and experimentally evaluated. The depth of the device within the micropod (given as a ratio relative to the micropod diameter) and the refractive index of the resin were critical parameters when determining the optoelectronic performance (Section S6 shows the effect of micropod size on the  $I_{\text{SC}}$  for SCs). In this work, the micropod geometry, size, and SC positioning were dictated by the design constraints to optimise the desirable properties (thickness and drapability) of the resultant fabrics. Therefore, a micropod diameter of 1.6 mm and a cell width of 1.5 mm was employed.

After covering the solar-micropod filament with a fibrous sheath, the  $I_{\text{SC}}$  and  $P_{\text{MAX}}$  values decreased by 29.3% and 32.5% (relative to

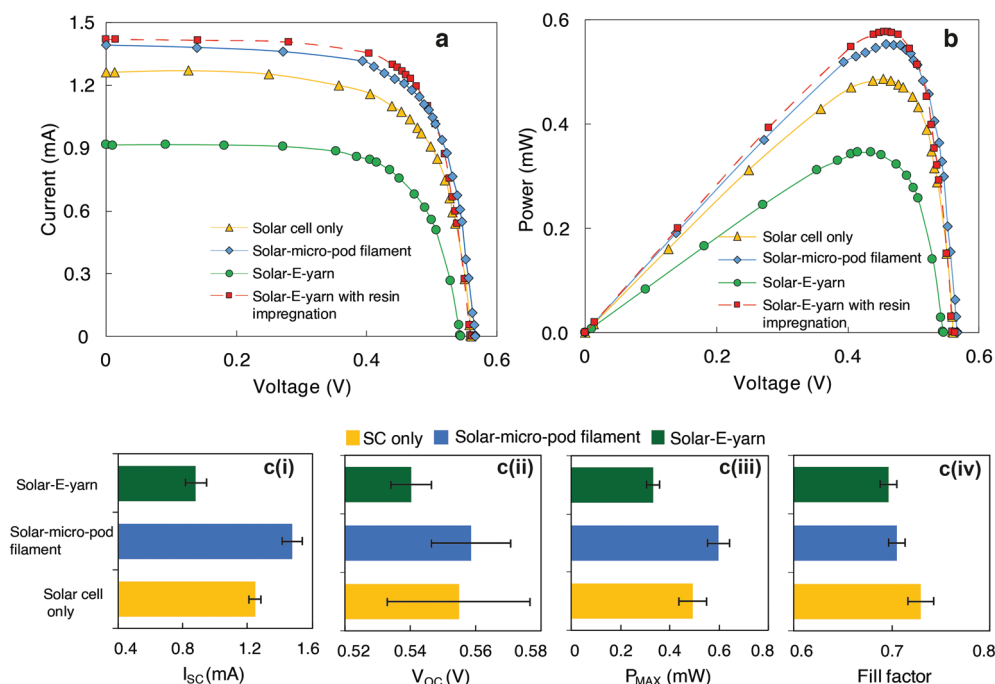


**FIGURE 3** Solar cell embedded yarn performance at different stages of the fabrication process. (A) Current–voltage (IV) characteristic curves, (B) power–voltage (PV) characteristic curves, (C(i)) short circuit current, (C (ii)) open circuit voltage, (C (iii)) maximum power output, and (C (iv)) fill factor. Error bars show the standard deviation of the results taken using five different samples [Colour figure can be viewed at [wileyonlinelibrary.com](http://wileyonlinelibrary.com)]

the values of bare SCs) due to reflectance and light absorbance effects of the fibrous sheath.  $V_{OC}$  did not change significantly due to the fabrication process, though FF was reduced by ~4.6%.

The intensity of light received by the SC within the solar-E-yarn was clearly affected by the fibrous sheath. Incident light could penetrate the fibrous sheath into the micropod in two ways: Firstly, the porous structure of the surrounding fibrous sheath would allow direct transmission of proportion of incident light through the structure without interference; secondly, light could diffuse through the fibrous sheath after interference. This light diffusion occurred by light scattering off of the fibre surfaces by partial reflection<sup>48</sup> and transmission through the fibre interiors (which absorbed a small proportion of the light). These interferences resulted in a reduction of light penetrating into the micropod and reaching the SC (shading effect), which is directly related to the fibre density of the sheath.<sup>61</sup> The theoretical study conducted previously<sup>48</sup> estimated that the effect of light scattering is more significant than light absorption. Use of textile fibres with lower delustrant<sup>62</sup> content can further decrease the light absorption while using lower number of thicker textile fibres or fibres with lower refraction index can minimise the effect of scattering (for example fluorinated polyesters or silicones could be used). These modifications will have implications on the light trapping effect, appearance, and hand-feel of the resultant fabrics; however, these modifications are not within the scope of this study.

When red- and black-coloured fibres were used for the fibrous sheaths (see Figure 4A), solar-E-yarns showed  $89.4 \pm 5.8\%$  and  $77.7 \pm 1.2\%$  of the normal solar-E-yarn (white sheath)  $I_{SC}$  value, respectively (Figure 4B). These experiments proved the viability of creating coloured solar-E-yarns without significantly compromising their performance. This also suggested that the light penetration into the resin micropod predominantly occurred through the spaces between the fibres.

### 3.2 | Solar cell embedded fabric construction and its performance

The solar energy harvesting fabric demonstrator generated  $P_{MAX}$  values of  $43.4 \pm 0.29$ ,  $31.00 \pm 0.38$ ,  $18.60 \pm 0.25$ , and  $7.62 \pm 0.17$

mW under 100%, 75%, 50%, and 25% of one sun illumination ( $100 \text{ mW/cm}^2$ , 1.5 AM spectrum), respectively, as shown in Figure 5A,C. At one sun intensity,  $I_{SC}$ ,  $V_{OC}$ , FF, and power density values of  $14.14 \pm 0.05 \text{ mA}$ ,  $5.14 \pm 0.02 \text{ V}$ ,  $0.598 \pm 0.004$ , and  $2.146 \pm 0.014 \text{ mW/cm}^2$  were observed, respectively (see Figure 5B,C). Overall, the  $I_{SC}$  and  $P_{MAX}$  values showed a close linear relationship with light intensity level, indicating a behaviour equivalent to a typical c-Si SC network.<sup>60</sup> The  $P_{MAX}$  per solar-E-yarn when woven into fabric was  $217.3 \mu\text{W}$ , ~4.5% lower than the average  $P_{MAX}$  values of 20 individual solar-E-yarns ( $227.5 \pm 17.5 \mu\text{W}$ ), owing to current/voltage mismatches caused due to cell-to-cell variations<sup>63</sup> and variations in angular position of the embedded SCs relative to the fabric's surface.

When worn, a solar energy harvesting fabric may undergo mechanical deformation; therefore, it is important to understand the effects of deformation on the electrical performance under these conditions. When subjected to shear deformation (Figure 5D), draping (Figure 5E), and bending (Figure 5F), the demonstrator fabric showed  $I_{SC}$  values of 13.83, 11.06, and 2.32 mA, respectively, under one sun intensity. These results provided clear evidence that the SC embedded fabric could generate power while undergoing various forms of deformation. The  $I_{SC}$  after bending significantly differed from the  $I_{SC}$  before deformation (14.14 mA), due to the lower surface area exposed to the light source (less than 30% of the photoactive area was exposed), which is also curved (incident angle varies across the exposed area). The modest reduction in  $I_{SC}$  after draping was due to the curvature of the photoactive area. There was an insignificant change in  $I_{SC}$  after shear deformation. These results indicated that the changes were likely caused by the change in incident angles, not due to electromechanical effects within the cells and cell network. The measured  $I_{SC}$  returned to normal after deformation in all cases. These results provide evidence of the viability of the solar-E-yarns for wearable applications where the clothing will be exposed to different levels of sunlight and has to undergo various mechanical deformations during its regular use.

The lengths of yarn used in the demonstrator shown in this work included a string of 10 SCs each; however, practically, this could be changed considering the required current, voltage outputs, and anticipated partial shading for a specific application. The E-yarn technology can be employed to embed any type of small semiconductor device (as demonstrated previously in the literature<sup>45,47,48,64</sup>) including bypass

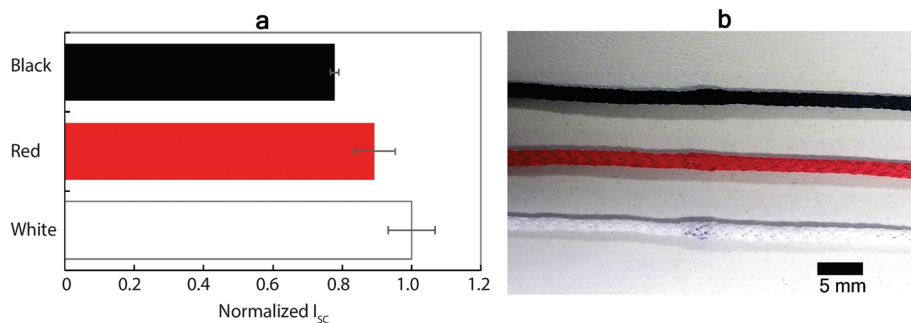


**FIGURE 4** Change in short-circuit current ( $I_{SC}$ ) output for solar-E-yarns with different colours of outer fibrous sheath. (A) Normalized  $I_{SC}$  values for  $1.5 \text{ mm} \times 1.5 \text{ mm}$  solar cells, embedded within 1.6-mm micropods, with white, red, and black fibrous sheaths of same fibre material and density. (B) Image of solar yarns with white, red, and black fibrous sheaths [Colour figure can be viewed at [wileyonlinelibrary.com](http://wileyonlinelibrary.com)]

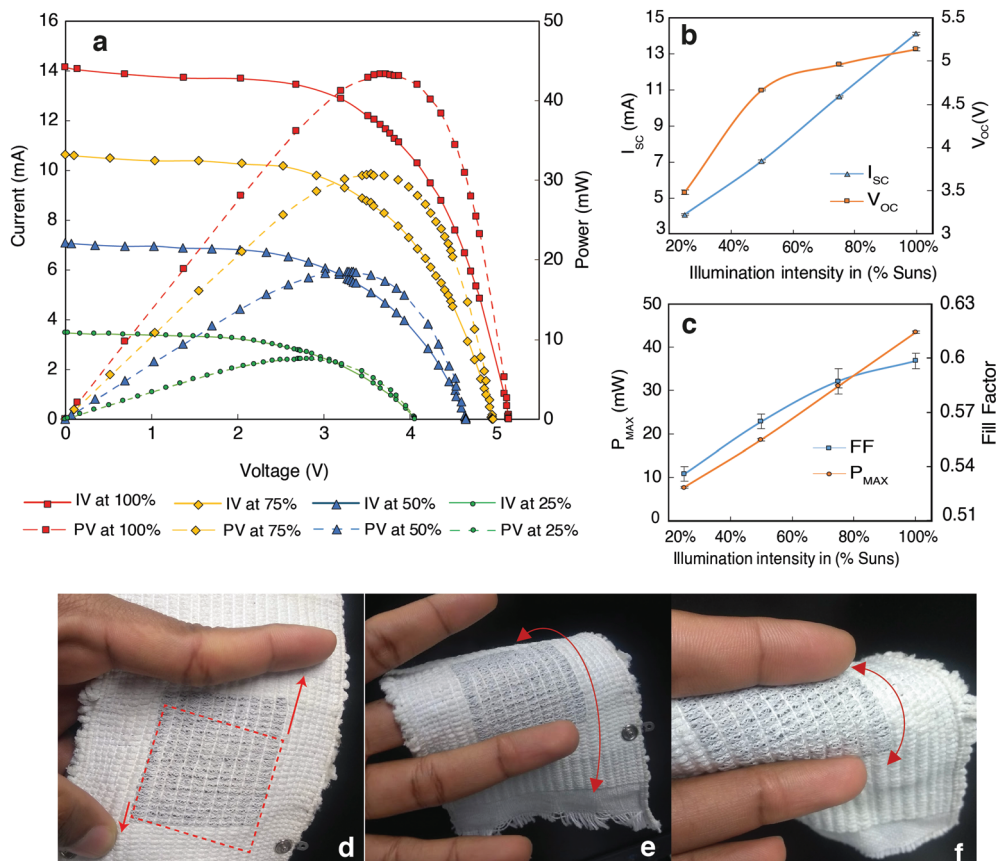


**FIGURE 5** Performance of solar cell embedded fabric demonstrator. (A) Current-voltage (IV) and power-voltage (PV) characteristics, (B) short circuit current ( $I_{SC}$ ) and open circuit voltage ( $V_{OC}$ ) and (C) fill factor (FF) and maximum power ( $P_{MAX}$ ) for solar cell embedded fabric demonstrator at different sun intensities (100% = one sun intensity with 1.5 AM standard solar spectrum). Error bars indicate the SD of five repeat experiments. Performance of the solar cell embedded fabric demonstrator under (D) shear deformation, (E) draping on a finger and (F) bending around a finger. Error bars show the standard deviation of five repeat measurements using one sample [Colour figure can be viewed at [wileyonlinelibrary.com](http://wileyonlinelibrary.com)]

diodes. Therefore, a bypass diode can be included at the end of each yarn (cell string) to minimise the potential effects of partial shading. While it may be vital to include bypass diodes to mitigate the adverse effects of partial shading, more specific information on a given application would be required to engineer an optimised E-yarn, hence this was beyond the scope of this paper.

The fabric demonstrator showed similar liquid moisture management characteristics (saturated water capacity of 17.43 g) to a control fabric sample (made from yarns without solar-micropod filaments, all other parameters remained constant), with a saturated water capacity of 17.29 g. The moisture transfer behaviour is crucial for the thermal comfort of the wearer, especially for activewear applications where the wearer generates sweat and heat while directly being exposed to warm conditions.

### 3.3 | Effects of change in the incident angle of light

During regular use, the angle of the incident light received by the solar fabric would change due to deformation of the fabric or movement of the user relative to the light source. It was therefore important to

understand and characterise the performance of the solar-E-yarns and resultant fabrics with different incident angles of light (Figure 6).

The change in  $I_{SC}$  was measured under one sun illumination for incident angles from  $0^\circ$  to  $180^\circ$  at different stages of the solar-E-yarn fabrication process normal to the longitudinal axis of the solar-E-yarn, as shown in Figure 6A. The bare SC showed  $I_{SC}$  values close to the theoretical values given by the cosine effect<sup>65</sup> from  $0^\circ$  to  $90^\circ$ , with negligible  $I_{SC}$  from  $90^\circ$  to  $180^\circ$  (ie, the SC was illuminated from the back side). The  $I_{SC}$  values for the solar-micropod filament increased by an almost constant amount ( $\sim 30 \mu\text{A}$ ) across all incident angles. This indicated that the convergent and light-trapping effects of the resin micropods were both significant and consistent at any incident angle. After covering the solar-micropod filament with the fibrous sheath, shading effects (reflectance and absorbance) at small incident angles (up to  $60^\circ$ ) were evident. Beyond  $60^\circ$ , the solar-E-yarn generated  $I_{SC}$  values higher than for the soldered SCs. Overall,  $I_{SC}$  for the solar-E-yarns exhibited less of a dependency on the incident angle of the light when compared with the SC only and solar-micropod filament. This result is highly desirable for wearable applications where the change in incident angle of the sunlight is dynamic and unpredictable.

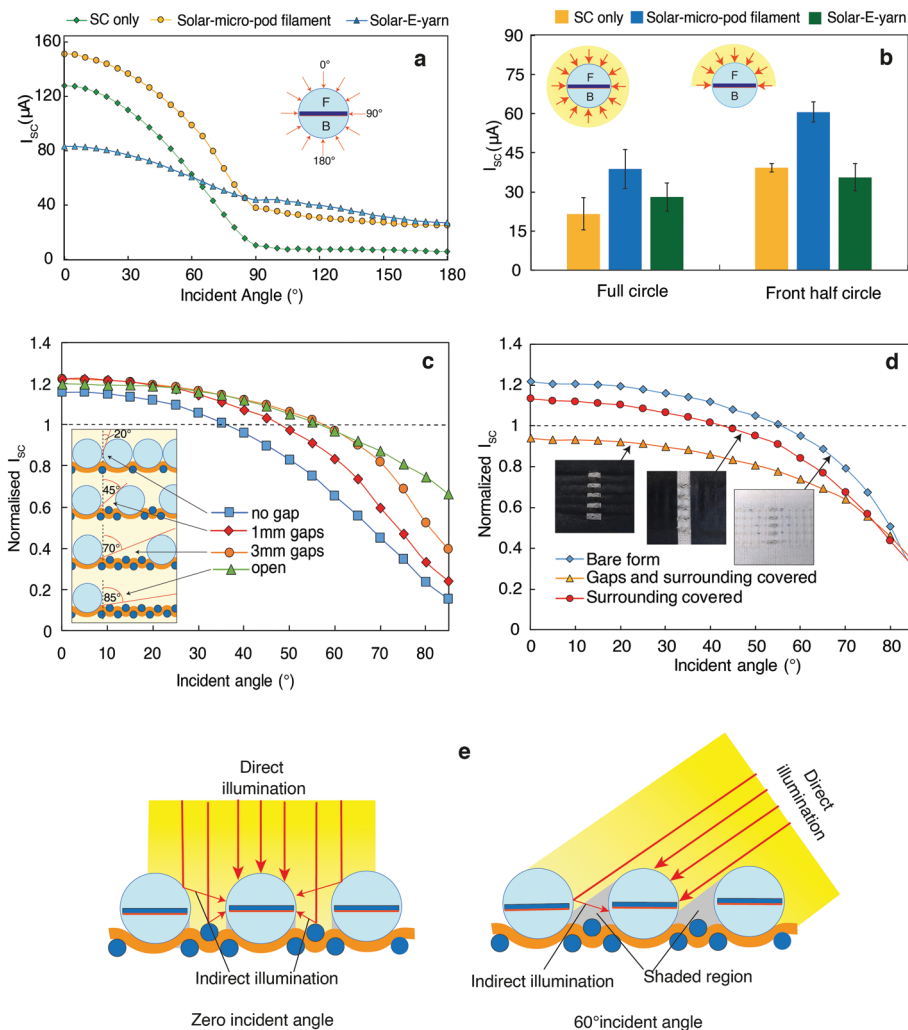


**FIGURE 6** Effect of incident angle on the performance of solar cell embedded yarns and fabrics. (A) Change in short circuit current ( $I_{sc}$ ) with the incident angle and (B) average  $I_{sc}$  of solar-E-yarns for front half circle and full circle exposure at different stages of the SC yarn fabrication process. (C) Change in the normalized  $I_{sc}$  (normalized to free-standing  $I_{sc}$  values) with incident angle for woven solar-E-yarns with different spacing between the solar-E-yarns. The box shows a schematic illustration of the cross section of the four fabric structures with different gaps between the solar-E-yarns: The light blue circles and dark blue circles representing solar-E-yarns and cotton weft yarns, respectively. Cotton warp yarns are shown in orange. In each case, the largest incident angle before shading from the adjacent yarn is indicated. (D) Change in normalized  $I_{sc}$  (normalized to free-standing  $I_{sc}$  values) with incident angle for woven solar-E-yarns with 3.0-mm spacing, when the surrounding of the solar-E-yarns area is changed with black, non-reflective tape. (E) Illustration of the effect of direct and indirect illumination received by woven solar-E-yarns at  $0^\circ$  and  $\sim 60^\circ$  incident angle. Error bars show the standard deviation of the results taken using five different samples. For (A), (C) and (D) graphs with error bars are shown in Section S7 for clarity [Colour figure can be viewed at [wileyonlinelibrary.com](http://wileyonlinelibrary.com)]

When the  $I_{sc}$  values were averaged across the front half circle ( $0^\circ$ – $90^\circ$ ) and full circle (see Figure 6B), the  $I_{sc}$  values for the solar-E-yarns were comparable with the  $I_{sc}$  values for the SC only. This behaviour can be attributed to the combined light trapping effects of the fibrous sheath and resin micropod at all incident angles (see Section S7 for further analysis).

The  $I_{sc}$  measurements conducted with the change in incident angle normal to the width direction of the embedded SC did not show a significant change at different stages of the solar-E-yarn fabrication process (the complete data set for the change in  $I_{sc}$  for different incident angles normal to the width direction of the embedded SC are included in Section S7). The results for the bare SC, solar-micropod filament, and solar-E-yarn approximately followed the cosine law.

The effects of the incident angle on the  $I_{sc}$  of the solar-E-yarns were then studied in fabric form in the orientation normal to the longitudinal axis of the solar-E-yarns, where multiple solar-E-yarns (each with one SC) were woven with different gaps between them, as shown in Figure 6C. Four conditions were explored: no gap, 1.0 mm and 3.0 mm gaps, and open (where the gap between the solar-E-yarns was over 20.0 mm). The  $I_{sc}$  values for the woven solar-E-yarns were normalised to the results from the free-standing solar-E-yarns.

In all of the cases explored, the solar-E-yarns within woven structures showed higher  $I_{sc}$  values than the corresponding free-standing values for small incident angles and lower  $I_{sc}$  values for higher incident angles. It is believed that this effect was due to the significant albedo effect<sup>66</sup> (light diffused by the surrounding and background) from the

surrounding fabric at smaller incident angles, as shown in Figure 6C. When the incident angle increased, the adjacent solar-E-yarn started to shade part of the incident light. By studying the cross-sectional geometry of the woven structure, it was clear that the angle at which the direct shading from yarns started to occur increased with the gaps size, which supported the experimental results. When the incident angle increased, the light flux to the solar-E-yarn reduced due to direct shading (from neighbouring solar-E-yarns) as well as a diminished albedo effect (as the gaps between the solar-E-yarns were also shaded); this is illustrated in Figure 6E.

The impact of the albedo effect due to the surrounding fabric was investigated empirically (Figure 6D) by covering the solar-E-yarn gaps (rectangular spaces on the fabric between the active regions of adjacent solar-E-yarns) and outer surrounding (complete surrounding except for the gaps). Experimental results using a woven sample with 3.0-mm gaps between the solar-E-yarns showed that the albedo enhancement from the solar-E-yarn gaps were higher and more angle dependent in comparison to the albedo enhancement by the outer surrounding. The albedo enhancement due to the gaps disappeared completely at incident angle of  $\sim 70^\circ$ , as estimated in the geometrical model demonstrated in Figure 6C.

These results suggested that woven fabrics with more distributed solar-E-yarn designs (ie, larger gaps between solar-E-yarns) are better suited for applications where dynamic incident angles are expected; while closely packed solar-E-yarn designs would give the best performance for applications with more predictable or small incident angles, or where the available surface area is limited. Additionally, a distributed yarn design would result in improved drapability; however, a detailed study of drapability was beyond the scope of this work.

### 3.4 | Durability testing

The wash durability of sets of five solar-E-yarns woven into fabrics was assessed using two washing methods. The first method used a domestic washing machine where one set of solar-E-yarns was washed with detergent inside of a wash bag in a 2-kg wash load and line dried. For the second method, a set of solar-E-yarns was hand washed with a detergent and line dried.

All of the solar-E-yarns functioned correctly (outputs comparable with the before wash values) after 15 machine wash cycles, with 60% of the E-yarns functioning correctly after 25 machine wash cycles. All of the hand-washed yarns functioned correctly after 25 hand wash cycles (Figure 7A). The wash durability can be attributed to three structural features of the solar-E-yarns and fabrics. Firstly, the discrete micropod structure protected the SCs from the water-detergent mix in the wash-bath and allowed some movement of the individual micropods within the E-yarns structure, as the micropods are not bound to the fibrous sheath. This allowed the E-yarn to bend and flex without structural failure of the fine copper wire interconnects occurring. Secondly, the fibrous sheath provided tensile reinforcement to the E-yarn. Finally, the fabric structure allowed the E-yarns to move independently (by shear deformation) under vigorous hydro-mechanical agitation.

The normalised  $I_{SC}$  and  $V_{OC}$  values (normalised to the before wash values as shown in Figure 7B) showed that the  $I_{SC}$  reduced by  $\sim 3\%$  and  $\sim 6\%$  after 25 hand wash and machine wash cycles, respectively. The FF values showed insignificant changes after 25 hand or machine washes. The  $P_{MAX}$  values showed  $\sim 13.5\%$  and  $\sim 10.4\%$  reduction after 25 machine wash cycles and 25 hand wash cycles (Figure 7C), which

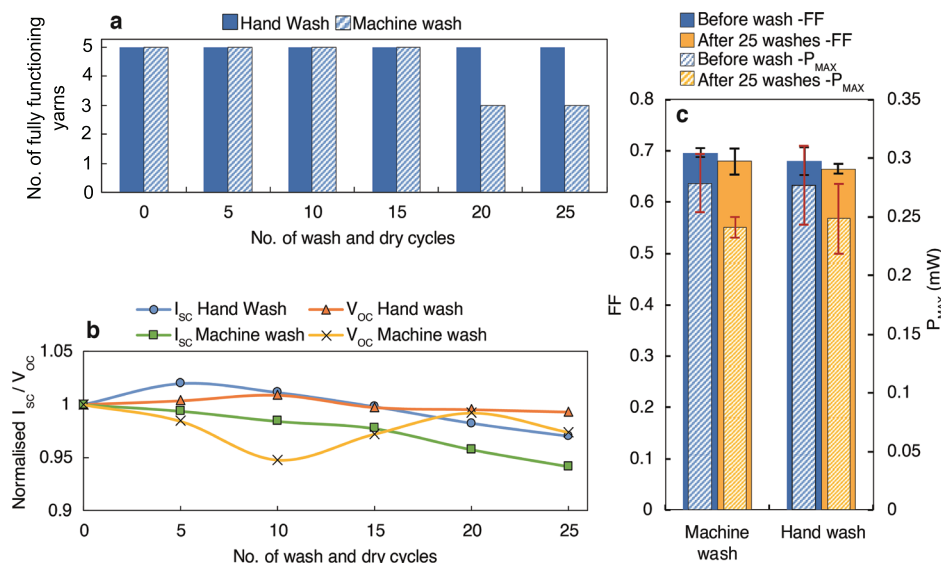


**FIGURE 7** Wash durability of solar-E-yarns embedded in woven fabrics. (A) Number of fully functioning solar-E-yarns after wash, (B) change in short circuit current ( $I_{SC}$ ) and open circuit voltage ( $V_{OC}$ ) after washing normalized to before wash values, and (C) change in fill factor (FF) and maximum power output ( $P_{MAX}$ ) after 25 wash cycles for machine washed and hand washed solar-E-yarns. Two sets of five solar-E-yarns woven into fabrics were tested for machine washing and hand washing. Average output of fully functioning solar-E-yarns indicated in (B) and (C) with error bars showing the SD of the full functioning solar-E-yarns in (C). For (B), graphs with error bars are shown in Section S8 for clarity. The absolute values for Figure 7B,C are provided in Section S8 [Colour figure can be viewed at [wileyonlinelibrary.com](http://wileyonlinelibrary.com)]

was the compound effect of changes in  $I_{SC}$ ,  $V_{OC}$ , and FF. The minor reductions in output power observed were possibly due to the redistribution of the textile fibres in the fibrous sheath during washing, which could increase the shading effect. Dissection of the broken solar-E-yarns confirmed that failures were due to the physical breakage of the copper wire interconnects outside of the resin micropods, as has been seen in earlier work<sup>48</sup> (see microscopic images in Section S8). The abnormal reduction in  $V_{OC}$  after 10 machine wash cycles may be due to an incomplete drying of the samples or change in ambient temperature during measurement.

Fabrics woven with solar-E-yarns, made using electrically insulated copper wires, were tested under one sun illumination. The insulated Cu wires employed in this experiment (BXL2001, OSCO Ltd, UK) had seven twisted strands of Cu, individually enamelled with Polyurethane coating. The electrical properties of these Cu wires were similar to the bare Cu wires used in the other experiments. The twisted strands were also covered with a Nylon fibre wrapping that protected the enamel from abrasion and reinforced the wires. These solar-E-yarns functioned correctly with a ~35% increase in  $I_{SC}$  when soaked with or immersed in liquid water, when compared with dry samples (see Figure 8A-8D). This can be explained by how water interacts with the textile fibres of the fibrous sheath as shown in Figure 8E.

The amount of light scattered by individual fibres in the sheath is related to the differences in refractive indices ( $\Delta n$ ) of the fibre material and the spaces between fibres. According to the Fresnel equation,<sup>67</sup> higher  $\Delta n$  will cause a higher amount of light scattering. When the solar-E-yarn is dry, the  $\Delta n$  value is 0.55 (refractive index of the fibre ~1.55, air 1). When the solar-E-yarn is wet, the  $\Delta n$  value is 0.22 (refractive index of water ~1.33). Due to lower amount of scattering

under wet conditions, the SC received a higher light flux, resulting in higher  $I_{SC}$  values. These results confirm that the SC embedded fabrics can generate power even under wet conditions.

Five solar-E-yarns woven into a fabric showed only a 5.6% reduction in  $I_{SC}$  after 6000 abrasion cycles (Figure 9A). Microscopic images confirmed that the solar-E-yarn surface fibres were redistributed due to abrasion, with an insignificant amount of surface fibre breakages (Figure 9B); this explains the change in performance after the abrasion cycles.

The results of the abrasion test confirmed that the solar-E-yarn embedded fabrics can withstand the washing and drying, mechanical rubbing, and wearing undergone by regular clothing without significantly altering their energy conversion capability. In addition, the results provided evidence of continuous functionality of the fabric under wet conditions, which is beneficial for outerwear.

### 3.5 | Demonstrating power generation capability

The ability of the SC embedded fabric demonstrator to charge three types of electrical device was explored, as ultimately the SC embedded fabric was designed to charge wearable devices. A 47-mF (5.5-V) supercapacitor (KEMET Electronic Components, USA) was charged using the solar fabric (under 100%, 75%, 50%, and 25% of one sun illumination); the supercapacitor reached its maximum voltage within 15 and 60 seconds under 100% and 25% sun intensity, respectively (Figure 10A).

Under 100% sun intensity, the fabric woven with solar-E-yarns was able to charge a 15-mAh (3.7-V) Li-ion battery to ~3.7 V within

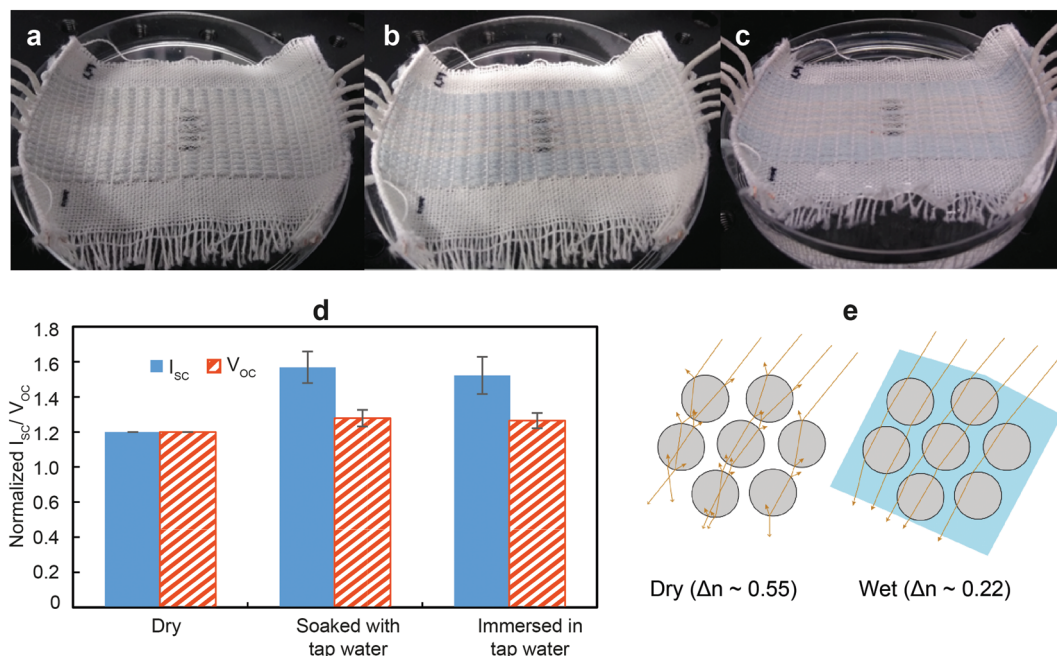


**FIGURE 8** Solar-E-yarn performance when soaked and immersed in tap water. Five solar-E-yarns constructed using electrically insulated copper wires woven into fabrics under (A) dry condition, (B) after soaking with tap water, and (C) after immersing in tap water. (D) The normalized  $I_{SC}$  and  $V_{OC}$  values for the five solar-E-yarns when dry, after soaking with tap water and after immersing in tap water. (E) An illustration representing the effect of water on the light transmission through the fibrous sheath of the solar-E-yarns [Colour figure can be viewed at [wileyonlinelibrary.com](http://wileyonlinelibrary.com)]

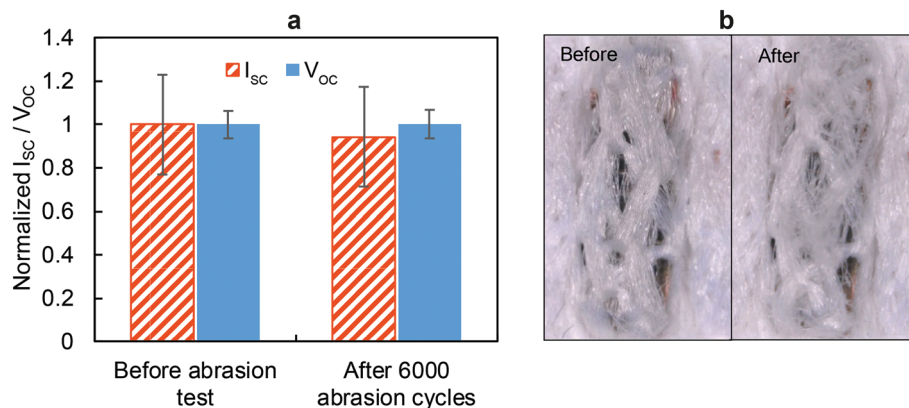


**FIGURE 9** Abrasion testing conducted on solar-E-yarns embedded in fabrics. Change in (A) performance and (B) appearance of solar-E-yarns in fabric form after 6000 abrasion cycles [Colour figure can be viewed at [wileyonlinelibrary.com](http://wileyonlinelibrary.com)]

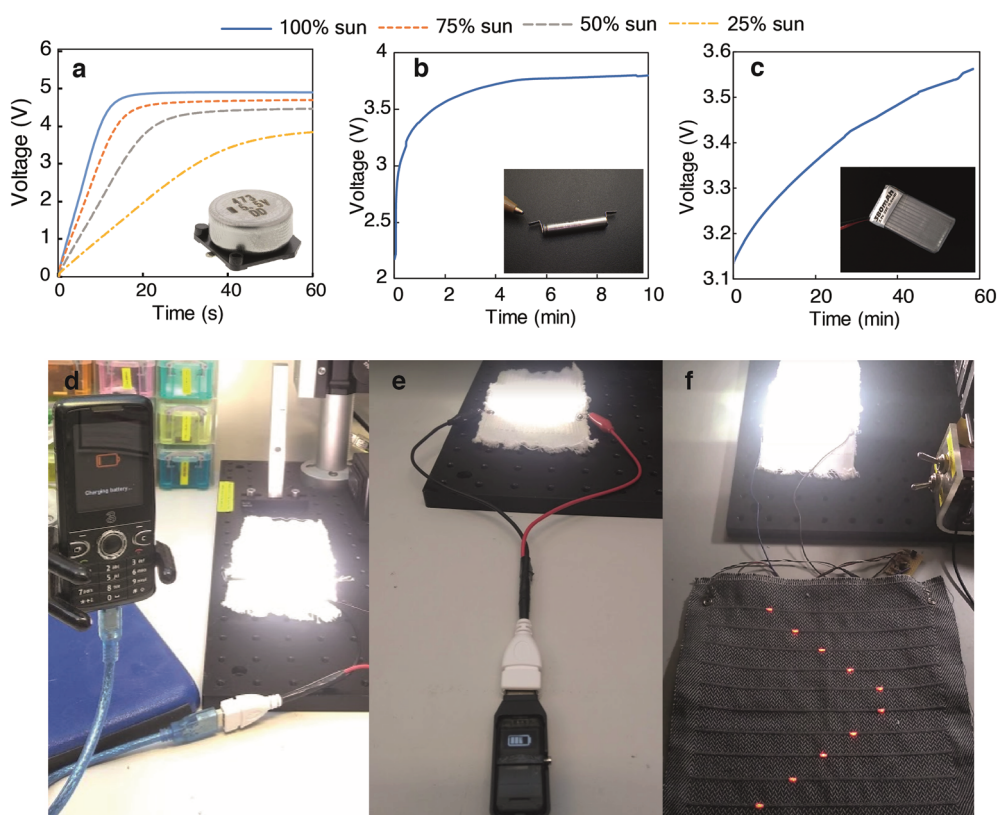


**FIGURE 10** Charging and powering devices using the solar cell embedded fabric. Evaluating the charging behaviour of (A) a 47-mF, 5.5-V super capacitor, (B) a 15-mAh, 3.7-V miniature Li-ion battery, and (C) a 380-mAh, 3.7-V Li-polymer battery using the miniature solar cell embedded fabric. Demonstrating the charging of (D) a basic mobile phone with a 1000-mAh, 3.7-V battery and (E) a fitness tracker with 50-mAh, 3.7-V battery and (F) powering an LED embedded fabric demonstrator developed using E-yarn technology<sup>45</sup> [Colour figure can be viewed at [wileyonlinelibrary.com](http://wileyonlinelibrary.com)]

10 minutes (Figure 10B), and charged a 380-mAh (3.7-V) Li-polymer battery from 3.1 to 3.55 V within 60 minutes (Figure 10C).

The SC embedded fabric was also capable of charging a basic mobile phone with 1000-mAh battery (Figure 10D, Supporting Video S1), a fitness tracker with a 50-mAh battery (Figure 10E, Supporting Video S2) and a LED fabric demonstrator (Figure 10F, Supporting Video S3) that contained 10 flashing LEDs (see Videos S1 to S3). These

demonstrations provide clear evidence of the utility of the solar energy harvesting fabric technology within regular clothing as a power source for wearable devices which have a power requirement around tens to few hundreds of milliwatts, which is typical for most wearable devices. It is envisioned that by employing advanced SC technologies such as bifacial cells and back contact cells the performance of the solar-E-yarns could be further enhanced in the future.

In a real-life scenario, the effects of a change in the incident angle, partial shading of the solar-E-yarn embedded regions, and change in incident light intensity are to be expected to occur. While the above demonstrations were not intended to comprehensively cover those scenarios, the characterisations conducted at varying light intensities (Section 3.2) and incident angles (Section 3.3), along with the demonstrations conducted under one sun intensity at direct exposure, should provide a complete understanding of the power generation capability of the solar fabrics prepared using the solar-E-yarns.

## 4 | CONCLUSION

Miniature SC embedded yarns, and resultant solar energy harvesting fabrics that possess the features of a textile fabric, have been presented for the first time. This new approach of integrating solar energy harvesting capability into fabrics is superior in aesthetic, textural, draping, and wash durability characteristics to the existing methods such as laminating, printing, or coating PV onto fabric surfaces, or weaving PV material coated wires or flexible PV tapes into fabrics. This desirable textile behaviour is rendered by the unique architecture of the SC embedded yarn fabricated using the electronic yarn technology. A solar energy harvesting fabric (active area 44.5 mm × 45.5 mm) that can generate 2.15 mW/cm<sup>2</sup> was demonstrated; this was sufficient to power a mobile phone. Solar cell embedded yarns were evaluated at different stages of their fabrication process. The inclusion of the SC within the resin micropod resulted in an increase in the output power due to convergent (lensing) and light-trapping effects. After covering with a fibrous sheath, the power output decreased due to reflectance and light absorbance effects. Durability tests have shown that SC embedded yarn incorporated fabrics can maintain their performance even after 15 domestic machine wash cycles, 25 hand wash cycles, and 6000 abrasion cycles. Research has shown that solar-E-yarns can be created in any colour, with only a minor effect on their performance. The study has revealed that in fabric form, larger gaps between SC embedded yarns will enhance the performance across a wider range of incident angles due to the albedo effect and reduced shading. This meant that the SC embedded yarn distribution within a fabric can be varied to achieve the optimum balance between angle independence and power density for a given application. The experimental results on power generation performance under various lighting conditions, for wash durability, moisture management behaviour, and conformability to three-dimensional shapes, validate the utility of the solution for regular clothing applications. These attributes will enable these solar fabrics to feature in future wearable electronics and electronic textiles to provide a continuous supply of power, without having to compromise on comfort, aesthetics, or wash durability.

## ACKNOWLEDGEMENTS

The authors would like to thank Carlos Oliveira for assistance in making E-yarns, Gayani Nandasiri and Richard Arm for support in preparation of moulds for soldering, Matholo Kgatuke and Daisy-Kate Hornsby for their assistance in preparing woven fabric samples, and

Arash Shahidi for the support in conducting abrasion and GATS testing. Achala Satharasinghe gratefully acknowledges Nottingham Trent University for funding the research.

## ORCID

Achala Satharasinghe  <https://orcid.org/0000-0002-7124-8228>

Theodore Hughes-Riley  <https://orcid.org/0000-0001-8020-430X>

## REFERENCES

- Piwiek L, Ellis DA, Andrews S, Joinson A. The rise of consumer health wearables: promises and barriers. *PLoS Med.* 2016;13(2):1–9 e1001953. <https://doi.org/10.1371/journal.pmed.1001953>
- Düking P, Hotho A, Holmberg H-C, Fuss FK, Sperlich B. Comparison of non-invasive individual monitoring of the training and health of athletes with commercially available wearable technologies. *Front Physiol.* 2016;7(71):1–11. <https://doi.org/10.3389/fphys.2016.00071>
- Sapargaliyev D. Learning with wearable technologies: a case of Google glass. In: Brown TH, van der Merwe HJ, editors. *Mob. Learn. Voyag.—From Small Ripples to Massive Open Waters. mLearn 2015*, Springer, Cham; 2015, p. 343–50. [https://doi.org/10.1007/978-3-319-25684-9\\_25](https://doi.org/10.1007/978-3-319-25684-9_25).
- Page T. A forecast of the adoption of wearable technology. *Int J Technol Diffus.* 2015;6:12–29. <https://doi.org/10.4018/IJTD.2015040102>
- Adapa A, Nah FF-H, Hall RH, Siau K, Smith SN. Factors influencing the adoption of smart wearable devices. *Int J Human-Computer Interact.* 2018;34:399–409. <https://doi.org/10.1080/10447318.2017.1357902>
- Magno M, Boyle D. Wearable energy harvesting: from body to battery. 2017 12th Int. Conf. Des. Technol. Integr. Syst. Nanoscale Era, IEEE; 2017, p. 1–6. doi:10.1109/DTIS.2017.7930169.
- Davis N. Powering wearables: battery types, current challenges, and energy harvesting—Power Electronics 2017. <https://www.powerelectronicsnews.com/technology/powering-wearables-battery-types-current-challenges-and-energy-harvesting> (accessed March 7, 2019).
- Jost K, Dion G, Gogotsi Y. Garment devices: integrating energy storage into textiles. In: Barfield W, editor. *Fundam. Wearable Comput. Augment. Real.* 2nd ed., CRC Press; 2015, p. 639–60. <https://doi.org/10.1201/b18703-29>.
- Bhatnagar V, Owende P. Energy harvesting for assistive and mobile applications. *Energy Sci Eng.* 2015;3:153–173. <https://doi.org/10.1002/ese3.63>
- Stoppa M, Chiolerio A. Wearable electronics and smart textiles: a critical review. *Sensors.* 2014;14(7):11957–11992. <https://doi.org/10.3390/s140711957>
- Zhu M, Huang Y, Ng WS, et al. 3D spacer fabric based multifunctional triboelectric nanogenerator with great feasibility for mechanized large-scale production. *Nano Energy.* 2016;27:439–446. <https://doi.org/10.1016/j.nanoen.2016.07.016>
- Pu X, Li L, Liu M, et al. Wearable self-charging power textile based on flexible yarn supercapacitors and fabric nanogenerators. *Adv Mater.* 2016; 28:98–105. <https://doi.org/10.1002/adma.201504403>
- Song S, Ahn Y, Yun KS. Scalable textile energy harvester in woven piezoelectric structures. 2015 Transducers—2015 18th Int Conf Solid-State Sensors, Actuators Microsystems, Transducers 2015 2015:708–9. <https://doi.org/10.1109/Tranducers.2015.7181021>.
- Torah R, Lawrie-Ashton J, Li Y, Arumugam S, Sodano HA, Beeby S. Energy-harvesting materials for smart fabrics and textiles. *MRS Bull.* 2018;43:214–219. <https://doi.org/10.1557/mrs.2018.9>

15. Leonov V. Thermoelectric energy harvesting of human body heat for wearable sensors. *IEEE Sens J*. 2013;13:2284-2291. <https://doi.org/10.1109/JSEN.2013.2252526>
16. Ylli K, Hoffmann D, Folkmer B, Manoli Y. Design, fabrication and characterization of an inductive human motion energy harvester for application in shoes. *J Phys Conf Ser*. 2013;476:12012. <https://doi.org/10.1088/1742-6596/476/1/012012>
17. International Energy Agency IEA. Solar Energy Perspectives. 2011. <https://doi.org/10.1787/9789264124585-en>.
18. Conibeer G, Willoughby A. *Solar Cell Materials: Developing Technologies*. New Jersey: Wiley Blackwell. 2014. <https://doi.org/10.1002/9781118695784>.
19. Schubert MB, Werner JH. Flexible solar cells for clothing. *Mater Today*. 2006;9:42-50. [https://doi.org/10.1016/S1369-7021\(06\)71542-5](https://doi.org/10.1016/S1369-7021(06)71542-5)
20. Mather R, Wilson J. Fabrication of photovoltaic textiles. *Coatings*. 2017;7:63. <https://doi.org/10.3390/coatings7050063>
21. Kumar M. Flexible photovoltaic textiles for smart applications. *Solar Cells - New Aspects and Solutions*. 2011. <https://doi.org/10.5772/19950>
22. van Dongen P. Wearable solar dress—Pauline van Dongen 2018. <http://www.paulinevandongen.nl/project/wearable-solar/> (accessed February 26, 2019).
23. Forbes. Tommy Hilfiger's solar-powered jacket—Wearable Tech in Review 2014. <https://www.forbes.com/sites/mitsubishiheavyindustries/2019/02/11/new-collar-manufacturing-a-new-fit-for-vietnam-as-a-next-generation-hub/#40fa21fc24f7> (accessed February 26, 2019).
24. Lin Y, Dong S, Li Z, et al. Energy-effectively printed all-polymer solar cells exceeding 8.61% efficiency. *Nano Energy*. 2018;46:428-435. <https://doi.org/10.1016/J.NANOEN.2018.02.035>
25. Bedeloglu A, Jimenez P, Demir A, Bozkurt Y, Maser W, Sariciftci NS. Photovoltaic textile structure using polyaniline/carbon nanotube composite materials. *J Text Inst*. 2011;102:857-862. <https://doi.org/10.1080/00405000.2010.525816>
26. Du P, Song L, Xiong J, Wang L, Li N. A photovoltaic smart textile and a photocatalytic functional textile based on co-electrospun TiO<sub>2</sub>/MgO core-sheath nanorods: novel textiles of integrating energy and environmental science with textile research. *Text Res J*. 2013;83:1690-1702. <https://doi.org/10.1177/0040517513490062>
27. Krebs FC, Biancardo M, Winther-Jensen B, Spanggaard H, Alstrup J. Strategies for incorporation of polymer photovoltaics into garments and textiles. *Sol Energy Mater Sol Cells*. 2006;90:1058-1067. <https://doi.org/10.1016/j.solmat.2005.06.003>
28. Zhao C, Liu Y, Beirne S, Razal J, Chen J. Recent development of fabricating flexible micro-supercapacitors for wearable devices. *Adv Mater Technol*. 2018;3:1800028. <https://doi.org/10.1002/admt.201800028>
29. Jung JW, Bae JH, Ko JH, Lee W. Fully solution-processed indium tin oxide-free textile-based flexible solar cells made of an organic-inorganic perovskite absorber: toward a wearable power source. *J Power Sources*. 2018;402:327-332. <https://doi.org/10.1016/J.JPOWSOUR.2018.09.038>
30. Nocito C, Koncar V. Flexible photovoltaic cells embedded into textile structures. In: Koncar V, editor. *Smart Text. their Appl*. 1st ed., Oxford: Woodhead Publishing; 2016, p. 401-22. <https://doi.org/10.1016/B978-0-08-100574-3.00018-7>.
31. Plentz J, Andr a G, Pliewischkies T, Br uckner U, Eisenhawer B, Falk F. Amorphous silicon thin-film solar cells on glass fiber textiles. *Mater Sci Eng B Solid-State Mater Adv Technol*. 2016;204:34-37. <https://doi.org/10.1016/j.mseb.2015.11.007>
32. Green MA, Hishikawa Y, Dunlop ED, et al. Solar cell efficiency tables (Version 53). *Prog Photovoltaics Res Appl*. 2019;27:3-12. <https://doi.org/10.1002/pip.3102>
33. Zhang Z, Li X, Guan G, et al. A lightweight polymer solar cell textile that functions when illuminated from either side. *Angew Chemie-Int Ed*. 2014;53:11571-11574. <https://doi.org/10.1002/anie.201407688>
34. Zhai S, Karahan HE, Wei L, et al. Textile energy storage: structural design concepts, material selection and future perspectives. *Energy Storage Mater*. 2016;3:123-139. <https://doi.org/10.1016/J.ENS.2016.02.003>
35. Li C, Islam MM, Moore J, et al. Wearable energy-smart ribbons for synchronous energy harvest and storage. *Nat Commun*. 2016;7:13319. <https://doi.org/10.1038/ncomms13319>
36. Yan J, Uddin MJ, Dickens TJ, Daramola DE, Okoli OI. 3D wire-shaped dye-sensitized solar cells in solid state using carbon nanotube yarns with hybrid photovoltaic structure. *Adv Mater Interfaces*. 2014;1(6):1-7. <https://doi.org/10.1002/admi.201400075>
37. Chai Z, Zhang N, Sun P, Huang Y, Zhao C, Fan HJ, et al. Tailorable and wearable textile devices for solar energy harvesting and simultaneous storage. *ACS Nano* 2016;acs.nano.6b05293. doi:<https://doi.org/10.1021/acsnano.6b05293>.
38. Li R, Xiang X, Tong X, Zou J, Li Q. Wearable double-twisted fibrous perovskite solar cell. *Adv Mater*. 2015;27(25):3831-3835. <https://doi.org/10.1002/adma.201501333>
39. Wang X, Kulkarni SA, Li Z, et al. Wire-shaped perovskite solar cell based on TiO<sub>2</sub> nanotubes. *Nanotechnology*. 2016;27:1-6. <https://doi.org/10.1088/0957-4484/27/20/20LT01>
40. Bedeloglu A, Demir A, Bozkurt Y, Sariciftci NS. A flexible textile structure based on polymeric photovoltaics using transparent cathode. *Synth Met*. 2009;159:2043-2048. <https://doi.org/10.1016/j.synthmet.2009.07.019>
41. Zhang Z, Yang Z, Deng J, Zhang Y, Guan G, Peng H. Stretchable polymer solar cell fibers. *Small*. 2015;11(6):675-680. <https://doi.org/10.1002/sml.201400874>
42. Jinno H, Fukuda K, Xu X, et al. Stretchable and waterproof elastomer-coated organic photovoltaics for washable electronic textile applications. *Nat Energy*. 2017;2(10):780-785. <https://doi.org/10.1038/s41560-017-0001-3>
43. Jeong EG, Jeon Y, Cho SH, Choi KC. Textile-based washable polymer solar cells for optoelectronic modules: toward self-powered smart clothing. *Energ Environ Sci*. 2019;12(6):1878-1889. <https://doi.org/10.1039/C8EE03271H>
44. Dias TK, Rathnayake A. Electronically functional yarns. GB259900B, 2017.
45. Hardy D, Moneta A, Sakalyte V, Connolly L, Shahidi A, Hughes-Riley T. Engineering a costume for performance using illuminated LED-yarns. *Fibers*. 2018;6:35. <https://doi.org/10.3390/fib6020035>
46. Lugoda P, Hughes-Riley T, Morris R, Dias T. A wearable textile thermograph. *Sensors*. 2018;18:2369. <https://doi.org/10.3390/s18072369>
47. Hughes-Riley T, Dias T. The development of acoustic and vibration sensing yarns for health surveillance. *25th Int Congr Sound Vib*. 2018;1-7.
48. Satharasinghe A, Hughes-Riley T, Dias T. Photodiodes embedded within electronic textiles. *Sci Rep*. 2018;8(1):16205. <https://doi.org/10.1038/s41598-018-34483-8>
49. Hughes-Riley T, Dias T. Developing an acoustic sensing yarn for health surveillance in a military setting. *Sensors*. 2018;18:1590. <https://doi.org/10.3390/s18051590>

50. Gibson PW. Factors influencing steady-state heat and water vapor transfer measurements for clothing materials. *Text Res J.* 1993;63:749-764. <https://doi.org/10.1177/004051759306301208>
51. Che X, Li Y, Qu Y, Forrest SR. High fabrication yield organic tandem photovoltaics combining vacuum- and solution-processed subcells with 15% efficiency. *Nat Energy.* 2018;3:422-427. <https://doi.org/10.1038/s41560-018-0134-z>
52. Feng J, Zhu X, Yang Z, et al. Record efficiency stable flexible perovskite solar cell using effective additive assistant strategy. *Adv Mater.* 2018;30:1801418. <https://doi.org/10.1002/adma.201801418>
53. Fraunhofer ISE. Photovoltaic trend: tandem solar cells record efficiency for silicon-based multi-junction solar cell—Fraunhofer ISE 2019. <https://www.ise.fraunhofer.de/en/press-media/press-releases/2019/photovoltaic-trend-tandem-solar-cells-record-efficiency-for-silicon-based-multi-junction-solar-cell.html> (accessed March 5, 2019).
54. Chen J, Huang Y, Zhang N, et al. Micro-cable structured textile for simultaneously harvesting solar and mechanical energy. *Nat Energy.* 2016;1:16138. <https://doi.org/10.1038/nenergy.2016.138>
55. Markvart T, Castañer L. Principles of solar cell operation. In: Markvart T, Castañer L, editors. *Pract. Handb. Photovoltaics*. 2nd ed., Elsevier Ltd; 2012, p. 7-31. <https://doi.org/10.1016/B978-0-12-385934-1.00001-5>.
56. Cruz-Campa JL, Okandan M, Resnick PJ, et al. Microsystems enabled photovoltaics: 14.9% efficient 14 micrometer thick crystalline silicon solar cell. *Sol Energy Mater Sol Cells.* 2011;95:551-558. <https://doi.org/10.1016/j.solmat.2010.09.015>
57. BSI Standards Publication. BS EN ISO 6330: 2012 Textiles—domestic washing and drying procedures for textile testing 2012. <https://shop.bsigroup.com/> ().
58. American Association of Textile Chemists and Colourists. AATCC M5 - Standardization of Hand Laundering for Fabrics and Apparel 2010:27709. <https://www.aatcc.org/wp-content/uploads/2015/01/M05-2007.pdf> (accessed January 15, 2019).
59. BSI Standards Publication. BS EN ISO 12947-2:2016—Determination of the abrasion resistance of fabrics by the Martindale method part 2: determination of specimen breakdown (ISO 12947-2:2016) 2016. <https://shop.bsigroup.com/> (accessed January 15, 2019).
60. Chegaar M, Hamzaoui A, Namoda A, Petit P, Aillerie M, Herguth A. Effect of illumination intensity on solar cells parameters. *Energy Procedia.* 2013;36:722-729. <https://doi.org/10.1016/j.egypro.2013.07.084>
61. Davis S, Capjack L, Kerr N, Fedosejevs R. Clothing as protection from ultraviolet radiation: which fabric is most effective? *Int J Dermatol.* 1997;36(5):374-379. <https://doi.org/10.1046/j.1365-4362.1997.00046.x>
62. Morton WE, Hearle JWS, Morton WE, Hearle JWS. Optical properties. *Phys Prop Text Fibres, Woodhead Publishing.* 2008;690-708. <https://doi.org/10.1533/9781845694425.690>
63. Kaushika ND, Rai AK. An investigation of mismatch losses in solar photovoltaic cell networks. *Energy.* 2007;32:755-759. <https://doi.org/10.1016/J.ENERGY.2006.06.017>
64. Hughes-Riley T, Lugoda P, Dias T, Trabi CL, Morris RH. A study of thermistor performance within a textile structure. *Sensors (Switzerland).* 2017;17(1804):1-14. <https://doi.org/10.3390/s17081804>
65. Mohanty P, Muneer T., Gago E.J., Kotak Y. Solar Radiation Fundamentals and PV System Components. In: Mohanty P, Muneer T., Kolhe M. (eds) *Solar Photovoltaic System Applications. Green Energy and Technology.* Springer, Cham. vol. 196. 2016. [https://doi.org/10.1007/978-3-319-14663-8\\_2](https://doi.org/10.1007/978-3-319-14663-8_2).
66. Brennan MP, Abramase AL, Andrews RW, Pearce JM. Effects of spectral albedo on solar photovoltaic devices. *Sol Energy Mater Sol Cells.* 2014;124:111-116. <https://doi.org/10.1016/J.SOLMAT.2014.01.046>
67. Keating MP. *Scattering, absorption, dispersion, and polarization BT—geometric, physical, and visual optics*, Butterworth-Heinemann; Burlington. 2002, p. 523-43. <https://doi.org/10.1016/B978-0-7506-7262-7.50027-8>.

## SUPPORTING INFORMATION

Additional supporting information may be found online in the Supporting Information section at the end of the article.

**How to cite this article:** Satharasinghe A, Hughes-Riley T, Dias T. An investigation of a wash-durable solar energy harvesting textile. *Prog Photovolt Res Appl.* 2019;1-15. <https://doi.org/10.1002/pip.3229>